Journal of
Composites Science

MDPI

Article

Functionalization of $BaTiO_3$ Nanoparticles to Optimize the Dielectric Performance of Electroactive Polymer Nanocomposites Based on PDMS Matrix

Nico Zamperlin [1,*], Alain Sylvestre [2], Alessandro Pegoretti [1], Marco Fontana [3] and Sandra Dirè [1]

[1] Department of Industrial Engineering, University of Trento, Via Sommarive 9, 38122 Trento, Italy; alessandro.pegoretti@unitn.it (A.P.); sandra.dire@unitn.it (S.D.)
[2] University Grenoble Alpes, CNRS, Grenoble INP G2Elab, 38000 Grenoble, France; alain.sylvestre@g2elab.grenoble-inp.fr
[3] Institute of Mechanical Intelligence, Sant'Anna School of Advanced Studies, Piazza Martiri della Liberta' 33, 56127 Pisa, Italy; marco.fontana@santannapisa.it
* Correspondence: nzamperlin@cicenergigune.com

Abstract

The growing demand for portable and wireless electronic devices, along with the necessity to reduce reliance on non-renewable energy sources, has driven the need for energy harvesting materials. Nanocomposites, combining a polymeric matrix and a high-performance dielectric ceramic phase, are a promising solution. In such systems, the design of a hybrid matrix–filler interface is critical for achieving desired properties. Here, nanocomposites (NCs) were prepared by adding various amounts of hydrothermally synthesized $BaTiO_3$ (BT) nanoparticles (NPs) to polydimethysiloxane (PDMS). To investigate hybrid interfaces, NPs were used either bare or surface-functionalized with two silanes, 3-glycidyloxypropyltrimethoxysilane (GPTMS) or 2-[acetoxy(polyethyleneoxy)propyl]triethoxysilane (APEOPTES). NC films (80–100 µm thick) were characterized by scanning electron microscopy (SEM), energy-dispersive X-ray spectroscopy (EDXS), and thermogravimetric analysis (TGA). Dielectric properties and breakdown strength (E_{BD}) were measured, and the theoretical volumetric energy density was calculated as a function of the filler loading and functionalization. The results demonstrate that hybrid interface design is pivotal for enhancing dielectric performance in NCs. APEOPTES-functionalized NPs significantly improved the dielectric response at a low filler loading (3.5%vol.), increasing permittivity from 2.8 to 7.5, E_{BD} from 33.8 to 42.1 kV/mm and energy density from 30 to >100 mJ/cm^3. These findings underscore that designing hybrid interfaces through NP functionalization provides an effective strategy to achieve superior dielectric performance in PDMS-based NCs, retaining the advantages of the elastomeric matrix by reducing the amount of ceramic fillers.

Keywords: polymer nanocomposites; PDMS; $BaTiO_3$; hybrid interfaces; organosilanes; dielectric materials

Academic Editor: Giuseppe Cavallaro

Received: 15 December 2025
Revised: 16 January 2026
Accepted: 19 January 2026
Published: 21 January 2026

1. Introduction

The increasing demand for wireless and portable electronic devices has led to a growing emphasis on energy harvesting and the use of high-performance dielectric materials [1–3]. These materials have gained significant attention due to their ability to convert mechanical stress or strain into electrical energy, offering promising applications in various

fields. Furthermore, materials for energy harvesting in the field of flexible and wearable electronics must combine good dielectric properties (high dielectric constant ε', high dielectric breakdown E_{BD}) with high flexibility. Ceramics, such as perovskitic oxides, are usually characterized by high values of ε'; unfortunately, they are rigid and fragile. On the other hand, polymers are flexible and present high values of E_{BD} but they have low permittivity and low electromechanical coupling factors. To overcome these issues, nanocomposites that combine the best characteristics of the two classes of materials have emerged as a valuable solution to address the inherent limitations of classic polymers and ceramics [4]. Nanocomposites, which comprise a polymer matrix combined with a high-performance dielectric ceramic phase, have shown significant improvements in dielectric and energy harvesting performance [5,6]. These enhancements include improved permittivity, superior thermal stability, and more efficient storable and convertible energy [7–9]. Several attempts have been made in recent years; for example Abinnas et al. [10] produced a mechanical nanogenerator with a dielectric permittivity of 9 and an output voltage of 0.8 V by dispersing bismuth titanate nanoparticles in a PDMS matrix. Nayak et al. [11,12] produced PDMS-$BaTiO_3$ nanocomposites and obtained a moderate increase in the dielectric constant from 4 to 6 using up to 41 wt%. of ceramic filler. In the development of polymer–ceramic nanocomposites for energy harvesting and dielectric applications, the design of the hybrid interface between the polymer matrix and the ceramic filler plays a crucial role in achieving the desired dielectric properties, namely high values of both relative permittivity and dielectric breakdown, to obtain materials able to exploit high energy densities. At the same time, dielectric losses must remain low or at least be contained in an effort to increase the dielectric constant. Various methods have been explored to modify this interface, including surface modification of the ceramic filler, polymer functionalization, and the use of coupling agents or compatibilizers [13–15]. These strategies aim to fine-tune the composite structure, thereby enhancing the overall performance of the composite material [16,17]. For example, Guan et al. [18] produced PDMS-$BaTiO_3$-CN nanocomposites, showing that the functionalization of barium titanate nanoparticles with carbon nanotubes (CN) using a silane coupling agent as a compatibilizer led to improved dielectric permittivity and a decreased dielectric loss. Zafar and Gupta [19,20] showed that controlling the particle morphology and dispersion thanks to the presence of functionalizing agents in epoxy-$BaTiO_3$ composites is one of the key factors to increase the permittivity. In addition to that, tuning the particle–matrix interface thanks to the presence of functionalizing agents could also be useful to tune the dielectric breakdown value, as shown by Li et al. [13]. According to the literature, among the functionalizing agents, organosilanes are widely used to improve the interface between the polymer matrix and the ceramic filler [21–24] because of their good reactivity and the wide commercial availability of compounds with different chain lengths, functional groups, and chemical characteristics, resulting in a wide range of properties [25]. By functionalizing the ceramic filler with organosilanes, the compatibility with the polymer phase is improved, leading to enhanced filler dispersibility. This results in several benefits for the composite material: the use of organosilanes that ensure a more uniform filler distribution within the polymer matrix [21,24] enhances the overall mechanical properties of the composite, such as tensile strength and toughness [23]; it is also possible to improve the interfacial bonding strength, promoting efficient stress transfer between the polymer and ceramic phases [21]. The functionalization with organosilanes can also enhance the thermal stability of the composite, preventing or delaying degradation at elevated temperatures [23]. Finally, the presence of organosilanes grafted on the filler surface can also modify the electrical AC conductivity and dielectric properties of NCs, as recently shown by Shanmugasundram [26] through the GPTMS functionalization of aluminum NPs incorporated into NCs made of polylactid acid/polyhydroxyalkanoate with intercalated montmorillonite. Accordingly, the

rational design of the hybrid interface appears as a powerful tool to enhance the dielectric performance of the final nanocomposites [24].

The present work aims to produce PDMS-$BaTiO_3$ (BT) nanocomposites with improved dielectric performances for possible application in energy harvesting, by exploring the effects on NC properties, such as NP dispersibility, permittivity, and dielectric breakdown, of both the ceramic filler content and functionalization. BT was functionalized with different organotrialkoxysilanes, namely 3-glycidyloxypropyl trimethoxysilane (GPTMS, G) and 2-[acetoxy(polyethyleneoxy)propyl] triethoxysilane (APEOPTES, A). The selected trialkoxysilanes bear organic chains of various lengths, with different steric and electron inductive properties, which in turn are expected to affect filler–matrix interactions. While GPTMS is widely used as a functionalizing agent, to the best of our knowledge, APEOPTES represents a novelty, combining the properties of silane coupling agents with the presence of highly polarizable polyethyelene oxide (PEO) groups in its chain. $BaTiO_3$ functionalization with PEO (or polyethylene glycol, PEG) was explored in the production of polyvinylidene fluoride (PVDF)-based composites [27] and proved to be beneficial for dielectric performance: APEOPTES combines the characteristics of PEO chains with the high reactivity for improved functionalization of silane coupling agents. The presence of a long PEO chain with a final polar end-chain group in the molecular structure of APEOPTES offers the possibility of forming a variety of weak interactions, such as van der Waals and London forces, with the PDMS chain. PEO chains are also expected to reduce filler–filler interactions that lead to the formation of $BaTiO_3$ clusters thanks to dipole–dipole interactions, and their intrinsic flexibility should allow for the improved embedding of NPs within the matrix. All these factors contribute to improving dispersibility and eventually the dielectric performance. By systematically studying the effects of tailoring the hybrid interface via silane functionalization, this research seeks to advance the understanding and development of nanocomposite materials for energy harvesting applications.

2. Materials and Methods

2.1. Materials

For the synthesis of BT NPs, reagent grade titanium (IV) isopropoxide $Ti(O^iPr)_4$ (Sigma-Aldrich, Saint Louis, MO, USA, CAS 546-68-9), barium acetate $Ba(CH_3COO)_2$ (Analyticals Carlo Erba, Milan, Italy, CAS 543-80-6), potassium hydroxide KOH (VWR International, Milan, Italy, CAS 1310-58-3), glacial acetic acid CH_3COOH (ITW Reagents, Darmstadt, Germany, CAS 64-19-7), and absolute ethanol C_2H_5OH (Merck KGaA, Darmstadt, Germany, CAS 64-17-5) were used. A 30%vol aqueous solution of hydrogen peroxide H_2O_2 (Merck KGaA, Darmstadt, Germany, CAS 7722-84-1) and deionized water (DI) were used for the hydroxylation of the particles. The reagents employed for the particles' functionalization were as follows: 3-glycidyloxypropyltrimethoxysilane (G) (Merck KgaA, Darmstadt, Germany, CAS 2530-83-8), 2-[(acetoxy(polyethyleneoxy)propyl]triethoxysilane (A) (Gelest, Morrisville, PA, USA), toluene C_7H_8 (Honeywell, Charlotte, NC, USA, CAS 108-88-3), n-hexane C_6H_{14} (Merck KgaA, Darmstadt, Germany, CAS 110-54-3), triethylamine Et_3N (TEA) (Merck KgaA, Darmstadt, Germany, CAS 121-44-8), and acetone $(CH_3)_2CO$ (Merck KGaA, Darmstadt, Germany, CAS 67-64-1). Wacker Silgel 612 A/B (Wacker Chemie AG, Munich, Germany) and pentane C_5H_{12} (Merck KGaA, Darmstadt, Germany, CAS 109-66-0) were employed for the composites' production. Kapton tape (Dupont, Wilmington, DE, USA), conductive copper tape, conductive aluminum tape, and PMMA (polymethylmetacrylate) sheets (purchased from RS Components Srl, Sesto San Giovanni, Italy) were used to produce composite films.

2.2. Synthesis and Functionalization of $BaTiO_3$ NPs

$BaTiO_3$ nanoparticles (labeled BTH) were produced by hydrothermal synthesis following the procedure reported in a previous study [28]. The functionalization of BTH nanoparticles was performed by applying the protocol described in a previous study [29]. In detail, BTH particles were first subjected to a hydroxylation process to increase the surface reactivity towards the functionalization reaction with two different organosilanes, GPTMS (G) and APEOPTES (A); the obtained particles were labeled BTH_G and BTH_A, respectively. The synthesis of BTH particles and their functionalization procedure are reported in details in the Supplementary Information, together with the molecular structure of the utilized organosilanes (Figure S1).

2.3. Production of PDMS-Based NCs

PDMS nanocomposites: Wacker Silgel 612 A (resin) was mixed with Wacker Silgel 612 A (hardener) in a weight ratio of 2:1 (3 g of A and 1.5 g of B) and 5 mL of pentane were added. Different amounts of BTH particles were added to obtain composites at 3.5 and 14%vol filler loading, similarly to the procedure described in previous work [29]. The obtained mixture was stirred for 1 h, sonicated, and further stirred until solvent evaporation. Once the solvent was evaporated, the mixture was applied to a PMMA substrate with Kapton-covered aluminum electrodes using a film applicator (Elcometer 4340 Automatic Film Applicator, Elcometer Ltd., Manchester, UK), with an application speed of about 3 cm/s producing films about 60–120 μm thick. The thickness of composites was measured both with a micrometer and a coating thickness gauge (Elcometer 456). The counter electrode built as the previous one was placed on the top with a spacer about 1 mm thick, and the films were cured at 80 °C for 90 min with the simultaneous application of an electric field of about 7 kV/mm. Self-standing films were obtained by gently detaching the produced layers from the substrates and characterized by the techniques reported in the next section. Films loaded with bare particles were labeled as Pf_3.5_BTH, and Pf_14_BTH (at low 3.5%vol and high 14%vol filler content, respectively); similarly, films loaded with A-functionalized and G-functionalized particles were labeled, respectively, as Pf_3.5_BTH_A, Pf_3.5_BTH_G, and Pf_14_BTH_G. Finally, to evaluate the effect of the fillers, a PDMS film sample, labeled as Pf_neat, was made under the same conditions. Filler content choice was performed on the basis of both previous internal studies and literature. The feasibility of adding higher volume fractions than the ones used in this work was explored, but did not give good results in terms of film formation. This led to the upper filler content being set at 14%vol. The low filler content was selected taking into account the experimental results and the literature; for example, Mandal et al. [30] observed a percolation threshold of $BaTiO_3$ particles of 100 nm in size of 5%vol in PVDF-based composites. Given that our particles were slightly bigger and functionalized, the low filler content was set at 3.5%vol (1/4 of the highest loading). Considering this, for that which concerns the A-functionalized samples, only the film with low BTH_A loading was characterized by the techniques reported in Section 2.4, due to defects in high loading films related to viscosity issues, which were unavoidable under the same experimental conditions used for all films. To explore the potential use of these composites as dielectric elastomer generators (DEG), the dielectric constant and dielectric breakdown of the samples were evaluated while they were in a deformed state. Slices of PDMS composite films were prepared and placed on paper frames; these frames were clamped and stretched to a stretching ratio of $\lambda = 2$ with a homemade apparatus as shown in Figure S2 of the Supplementary Information. The central portion of the stretched samples was clamped on rigid Cu-covered epoxy substrates, serving as the bottom electrode, while Au-electrode was sputtered on the top to perform dielectric spectroscopy and dielectric breakdown measurements to assess the impact of stretching

on the samples. All the samples are reported in Table 1 with their respective labeling and compositions.

Table 1. Sample labeling, thickness, and composition.

Sample Label	Thickness (μm) Std. Dev. (-)	Filler Type	Filler Content (%vol.)	Functionalizing Agent
Pf_neat	75 (3)	No filler	0	No functionalizing agent
Pf_3.5_BTH	65 (4)	Bare BTH NPs	3.5%vol.	No functionalizing agent
Pf_3.5_BTH_G	55 (3)	Functionalized BTH NPs	3.5%vol.	GPTMS
Pf_3.5_BTH_A	65 (4)	Functionalized BTH NPs	3.5%vol.	APEOPTES
Pf_14_BTH	120 (10)	Bare BTH NPs	14%vol.	No functionalizing agent
Pf_14_BTH_G	85 (8)	Functionalized BTH NPs	14%vol.	GPTMS

2.4. Characterization

Thermogravimetric Analysis (TGA) curves of composite films were collected with a TA Instruments TGA Q5000 (New Castle, DE, USA) between 30 and 700 °C and a heating rate of 10 °C/min in flowing air to evaluate the thermal stability of the composites. For Field Emission Scanning Electron Microscopy (FE-SEM): the composites were analyzed with a Carl Zeiss (Carl Zeiss S.p.A., Milan, Italy) Gemini Supra 40 Field Emission Scanning Electron Microscopy (FE-SEM) using secondary electrons (SE) as the main signal with the following parameters: accelerating voltage 7.5–10 kV at 20,000×, 10,000×, 5000×, 2000×, and 1000×. Before imaging, samples were metal-sputtered with a Q150T coater (Quorum Technologies Ltd., London, UK) with Pt/Pd-80/20 alloy. Energy Dispersive X-Ray Spectroscopy (EDXS): EDXS images were collected on composites with a Jeol JSM-5500 SEM equipped with an EDXS detector and an operating voltage of 20 kV at 2000×, 1000×, and 500× magnification.

The evaluation of the dielectric constant (ε′) and breakdown strength (E_{BD}) is of importance to evaluate the potential energy-storage performances of the composites. Dielectric Spectroscopy (DS) measurements were performed using Novocontrol technologies Alpha-A High-Performance Frequency Analyzer (Novocontrol Technologies GmbH & Co. KG, Montabur, Germany). Wide frequency [10^{-2} Hz–10^{6} Hz] and temperature [−140–+120 °C] ranges have been explored on composite films, providing both extensive dielectric data on these materials and covering application fields ranging from cryogenic to heating of electroactive polymers under extended frequency excitation conditions. For DS measurements, sputtered 200 nm thin gold electrodes were deposited for a metal–insulator–metal configuration and an ac-voltage in the range of 1–3 V was applied to the structure (the amplitude of this voltage does not affect the dielectric response in these conditions of experiments and sample specifications). The thickness of the composite films was well controlled, and the samples were in the 60–120 μm range. For measurements at high/low temperature: 3 washing cycles with nitrogen (vacuum + N_2 filling) were performed prior to the measurement to remove humidity. The dielectric constant ε′ is one of the most crucial quantities as it is linked to the ability of a material to store electrical energy. Dielectric losses ε″ and AC conductivity σ′ constitute other parameters of interest for estimating material leakage and its suitability for integration into applications.

The E_{BD} of the composite films was evaluated by placing the film between a top ball electrode connected to the high voltage and a grounded bottom electrode; see Figure S3. The voltage was increased with a ramp of 50 V/s (using a Keithley 3390 oscilloscope as wave generator coupled with a Keithley 2290-5 5 kV as generator, Keithley Instruments, Solon, OH, USA) until dielectric failure; 15 measurements per sample were recorded. The relative permittivity ε′ of the materials and the breakdown strength allowed us to

estimate the theoretical volumetric energy density that can be stored in the films, which was calculated using the equation $U = \frac{1}{2}(\varepsilon_0 \varepsilon' E_{BD}^2)$. To explore the potential use of these composites as dielectric elastomer generators, the same properties were evaluated while they were in a deformed state (see Supplementary Information).

3. Results and Discussion

In a previous work [28], the functionalization of BT NPs (BTH, mean size 120 nm) prepared by an optimized hydrothermal synthesis was studied in detail. The reaction of BTH with both GPTMS and APEOPTES resulted in a higher degree of surface functionalization for BTH_G with respect to BTH_A, due to steric and electron-inductive effects. Epoxy- and PDMS- based nanocomposites with bare and functionalized $BaTiO_3$ NPs were prepared in form of disks by solvent-casting, highlighting the beneficial effect of functionalization for improving NP dispersibility [29].

This research investigates the potential of PDMS-based nanocomposite self-standing films for applications as electroactive elastomers in the context of energy harvesting. The effects of ceramic filler loading (3.5 and 14%vol) and NPs functionalization with GPTMS on microscopic features, thermal stability, electrical AC conductivity, and dielectric properties of composite films were studied in detail. To investigate the impact of filler–matrix hybrid interfaces on dielectric performance while reducing the effects due to filler–filler interactions, a composite film containing 3.5%vol of NPs functionalized with APEOPTES, a PEO-based organosilane, was prepared. Its properties were compared to those of analogous samples prepared with bare and G-functionalized particles.

3.1. Microstructural and Thermal Characterization

All samples are free of significant macroscopic defects or pores and the surfaces are homogeneous; the self-standing films are very flexible with thicknesses of around 60–80 μm for Pf_neat and 3.5%vol loaded samples (Table 1), independently of the functionalization while the thickness of samples loaded with 14%vol of filler is in the range of 120 μm (Table 1); the higher viscosity of the starting polymer–ceramic solution at high filler contents results in a lower homogeneity during the film deposition, and, consequently, in a higher final thickness. The SEM micrographs displayed in Figure 1 provide valuable insights into the cross-section of the PDMS film composites. Remarkably, all samples exhibit an absence of defects and bubbles and a smooth surface of the cross-section. SEM analysis confirms, as reported in Table 1, that the highly loaded samples, namely Pf_14_BTH and Pf_14_BTH_G, demonstrate a higher thickness compared to the others. It is worth noting that samples containing bare particles, such as Pf_3.5_BTH and P_14_BTH, reveal the presence of large particle agglomerates measuring several tenths of microns. Conversely, the inclusion of functionalized particles in the composite (Pf_3.5_BTH_G and Pf_14_BTH_G) results in a significantly enhanced dispersibility: no prominent agglomerates are visible, and particles appear to be well separated within the matrix. Likewise, the sample Pf_3.5_BTH_A, prepared with A-functionalized NPs, shows very well-dispersed particles. A tendency to align towards the direction of the applied electric field with the formation of the particles' filaments was observed in a previous work on disk samples of the same composition prepared by casting [29]. In this case, no alignments were observed, and this effect is probably due to the different film fabrication procedure, which produces much thinner samples, thus allowing a fast crosslinking reaction. The slight inconsistencies in thickness between data reported in Table 1 (evaluated by a thickness gauge that foresees the application of a small force on top of the films) and the SEM images (Figure 1) could be due to both the different techniques used and the preparation method of the SEM specimens (the films were cooled

in liquid nitrogen and subjected to brittle fracture), which can cause deformation in very thin films.

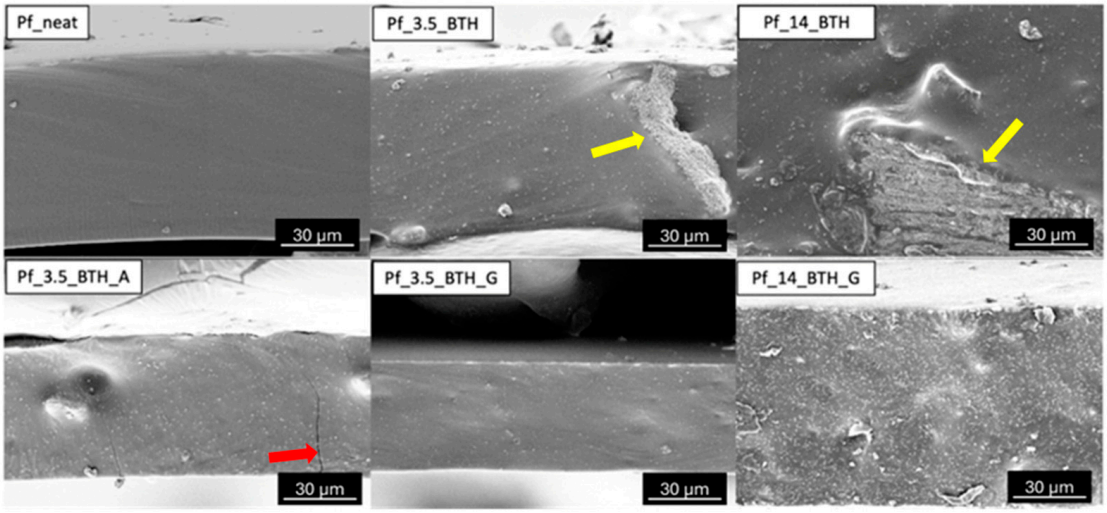

Figure 1. Cross-sections of PDMS-based composites with different functionalized fillers. Yellow arrows indicate large agglomerates in composites with bare BTH particles. The red arrow indicates a crack formed during liquid nitrogen cracking for the cross-section evaluation.

The improved dispersibility with NP surface functionalization is further supported by the images reporting Ba elemental maps of PDMS-based composites (Figure 2). The samples with bare particles, PF_3.5_BTH and Pf_14_BTH, show large agglomerates (in the range 10–15 µm), visible from the more intense yellow spots combined with depletion regions (black regions); this occurs particularly in the case of the sample at 14%vol filler loading. It is worth noting that with the particles being submicrometric in size (≈120 nm), with a narrow distribution and spherical shape, their spontaneous tendency to form agglomerates is quite high. The use of G-functionalized particles leads to a reduction in both the number and size of agglomerates. However, a few agglomerates are still present, which could also be influenced by the eventual ring-opening reactions of the GPTMS oxyrane rings that could lead to aggregate formation by crosslinking among the particles; this occurs more easily in Pf_14_BTH_G. A-functionalized particles demonstrate even better control over the interface. In fact, the polar ether groups of the PEO chains present in APEOPTES can form weak interactions, such as van der Waals forces as well as London's dispersion forces, with the PDMS matrix, according to reported mechanisms in polymer nanocomposites [31–33]. Furthermore, the presence of a much longer and flexible organic chain likely facilitates the formation of a more homogeneous hybrid interface and the stabilization of particles within the siloxane matrix. The presence of a more homogeneous hybrid interface together with the aforementioned weak interactions between the silane and the PDMS matrix promotes a more uniform dispersion of particles throughout the composite, highlighting the role of hybrid interfaces in controlling filler dispersion.

Thermogravimetric curves were collected to evaluate the thermal stability of the composites as shown in Figure S4 together with their associated results in Table S1. The thermogravimetric curve of Pf_neat in air shows two steps: the first centered around 356 °C; and the second at higher temperatures, around 465 °C. This double-step process has already been reported in the literature [24] and ascribed to a first decomposition of the PDMS chain that competes with an oxidative crosslinking, which contributes to stabilizing the material, while further decomposition occurs above 400–450 °C. The addition of bare BTH nanoparticles increases the thermal stability of the composites by shifting the flex point towards higher temperatures; the first loss temperature moves to 385 °C for Pf_3.5_BTH

and to 401 °C for Pf_14_BTH. This effect is more evident when particles are functionalized with GPTMS; in fact, the first weight loss is centered at 411 °C for Pf_3.5_BTH_G and 431 °C for Pf_14_BTH_G. Concerning the second weight loss of Pf_3.5_BTH_G, it is shifted at 517 °C with respect to the 499 °C of the samples filled with bare particles (Pf_3.5_BTH). No second loss is found for Pf_14_BTH_G as in Pf_14_BTH. Finally, looking at the A-functionalized sample, the first loss is further shifted towards higher temperatures being centered at 390 °C, very similar to that of the G-functionalized sample, and the second loss occurs around 504 °C. These results highlight the additional beneficial effect provided by particle functionalization—and interface engineering—in improving the thermal stability of the samples. The FTIR spectra of the PDMS-based nanocomposites were also collected and they are showed in the Supplementary Information with a brief comment (Figure S5).

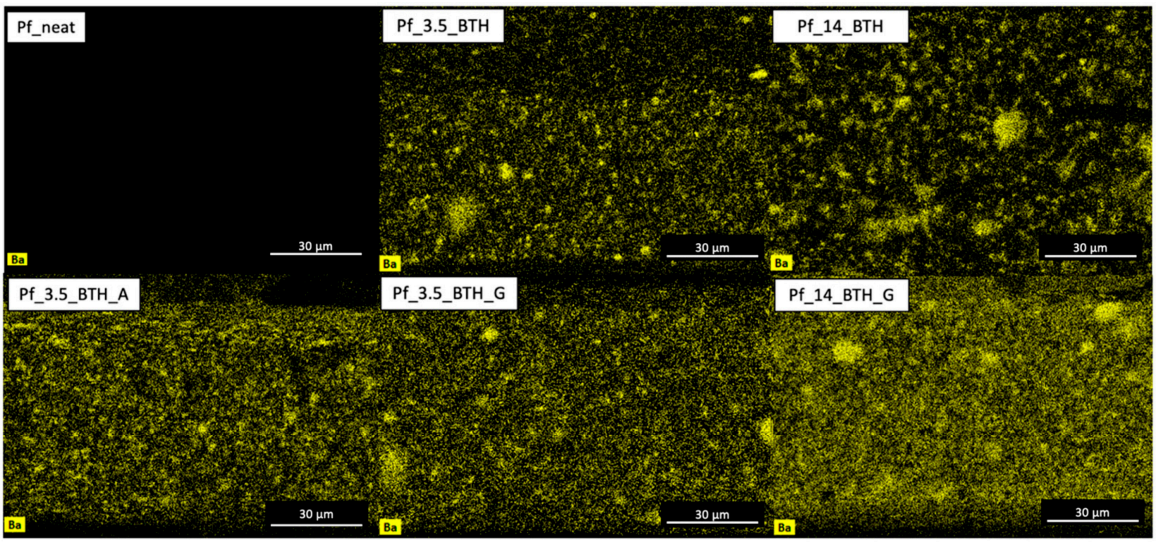

Figure 2. EDXS Ba elemental map of PDMS-based composite films.

3.2. Electric and Dielectric Characterization

3.2.1. Dielectric Spectroscopy (DS)

DS is widely used for the study of dielectric properties and it could be particularly useful when dealing with composite materials [34,35]. Figure 3 displays the real part of the dielectric constant of composites films together with one of the ceramic pellets produced with the BTH particles for the sake of comparison. The neat PDMS matrix has a permittivity of 2.7, matching the technical data sheet, while BTH powders exhibit a permittivity of around 1000 at high-frequency (Figure 3). As expected, incorporating BTH powders into PDMS increases the permittivity, over the entire frequency range, and the extent of this effect depends on the filler amount [36–38]. Compared to studies in which strontium titanate is added to a silicone matrix [38], it is clear that choosing barium titanate has the advantage of significantly increasing the dielectric constant while maintaining low losses and low AC conductivity. This is evidenced by the increase in the permittivity value going from Pf_neat to Pf_3.5_BTH and Pf_14_BTH. This enhancement is due to the increase in the relative ratio between materials with a high dielectric constant (BT) and with a low dielectric constant (PDMS). The surface functionalization of filler particles with GPTMS further enhances the permittivity, and this effect is evident in Pf_3.5_BTH_G and even more in the highly loaded samples. This increase in permittivity with GPTMS functionalization is clearly visible across the entire frequency range, particularly at the highest frequencies investigated (1 MHz). This indicates that this increased permittivity is the result of polarization mechanisms occurring at much higher frequencies, but is

also due to the polar nature or polar groups' promoting nature of reagents employed for particles' functionalization. It can therefore be argued that the functionalization applied promotes ionic (i.e., molecular) and possibly electronic polarization mechanisms. It is worth noting that the material with the highest dielectric constant (Pf_14_BTH_G) shows a permittivity that increases at the lowest frequencies below one hertz. This trend is also present (but difficult to observe on the scale of the chosen figure) for Pf_14_BTH. Two effects can be put forward to explain this trend. Adding a larger amount of BTH will promote a specific surfaces area (SSA) between the BTH and the PDMS. This will therefore promote interfacial polarization mechanisms, which will result in an increase in permittivity from a dielectric point of view. This interfacial polarization mechanism can be accentuated if the electrical conduction of free charges takes place. It can be seen that the functionalization of the particles reinforces these possibilities. To be thorough, when reducing the frequency, interfacial polarization dominates the permittivity curve of the BTH pellets due to numerous particle–particle interfaces, and the ceramic fillers' dielectric properties vary based on factors like grain size and microstructural features [39–41]. Finally, we do not want to rule out the possibility that enhancing matrix–filler interfaces with organosilanes triggers dipolar polarization due to polar groups in the molecular chain. This also enhances the Maxwell–Wagner–Sillars (MWS) [42] interfacial interaction at the particle–matrix interface, leveraging the interfacial polarization phenomenon [43,44]. It is interesting to note that films containing 3.5% of both BTH_G and BTH_A exhibit no significant differences in permittivity, with base values of about 7.6 and 7.1, respectively. Therefore, replacing GPTMS with APEOPTES preserves the advantages of the hybrid interface in terms of permittivity. Compared to recent works on composite BT_PDMS and other PDMS composites [45–47], the addition of functionalized BTH NPs, in our case, allows for much higher dielectric constant values, with a good stability in the whole frequency range investigated.

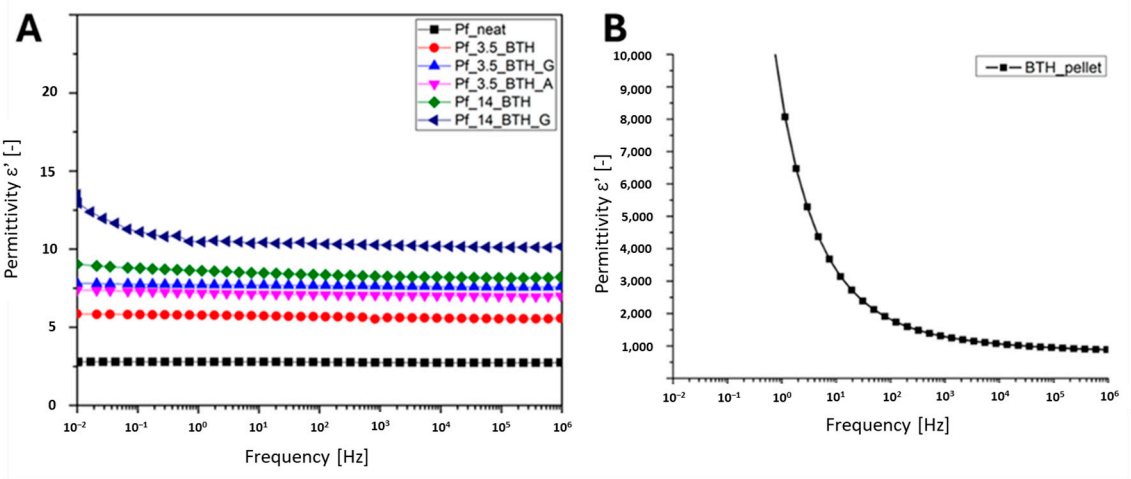

Figure 3. (**A**) Real part of permittivity for PDMS-based films as a function of the frequency; (**B**) real part of permittivity for BTH powder pellets for the sake of comparison.

Temperature's influence on the dielectric constant has been studied, revealing distinct trends in permittivity frequency sweeps at various temperatures (Figure 4). Pure PDMS is amorphous above −40 °C, with a glass transition temperature of approximately −125 °C and cold crystallization temperature around −90 °C, depending on conditions and PDMS type [48–50]. Increasing temperature causes a slight decrease in permittivity, following the trend commonly observed in apolar materials according to the Langevin theory [51]. High temperatures enhance low-frequency polarization, starting at higher frequencies. The addition of particles leads to a frequency-dependent decrease in permittivity, as the

polarization levels off and the dipoles struggle with rapid field alternation. This effect intensifies at higher temperatures, possibly due to thermal excitation. At lower filler content, particle–particle interactions appear less significant than particle–macromolecule interactions. The significant low-frequency increase in G-functionalized samples at high temperatures may stem from other phenomena related to the molecular structure of the functionalizing agent; in fact, the GPTMS chain is relatively short and could be thermally excited increasing its mobility by increasing the temperature [52]. The effect is more pronounced for Pf_14_BTH_G with respect to Pf_3.5_BTH_G because of the higher amount of particles and consequently of the organosilane. In Pf_3.5_BTH_A, the effect is less evident if compared with Pf_3.5_BTH_G and this could be due to the different molecular structure and chain length of A with respect to G. With APEOPTES, the presence of conductive PEO units at the hybrid interface could activate specific conduction mechanisms at elevated temperatures, further influencing dielectric behavior.

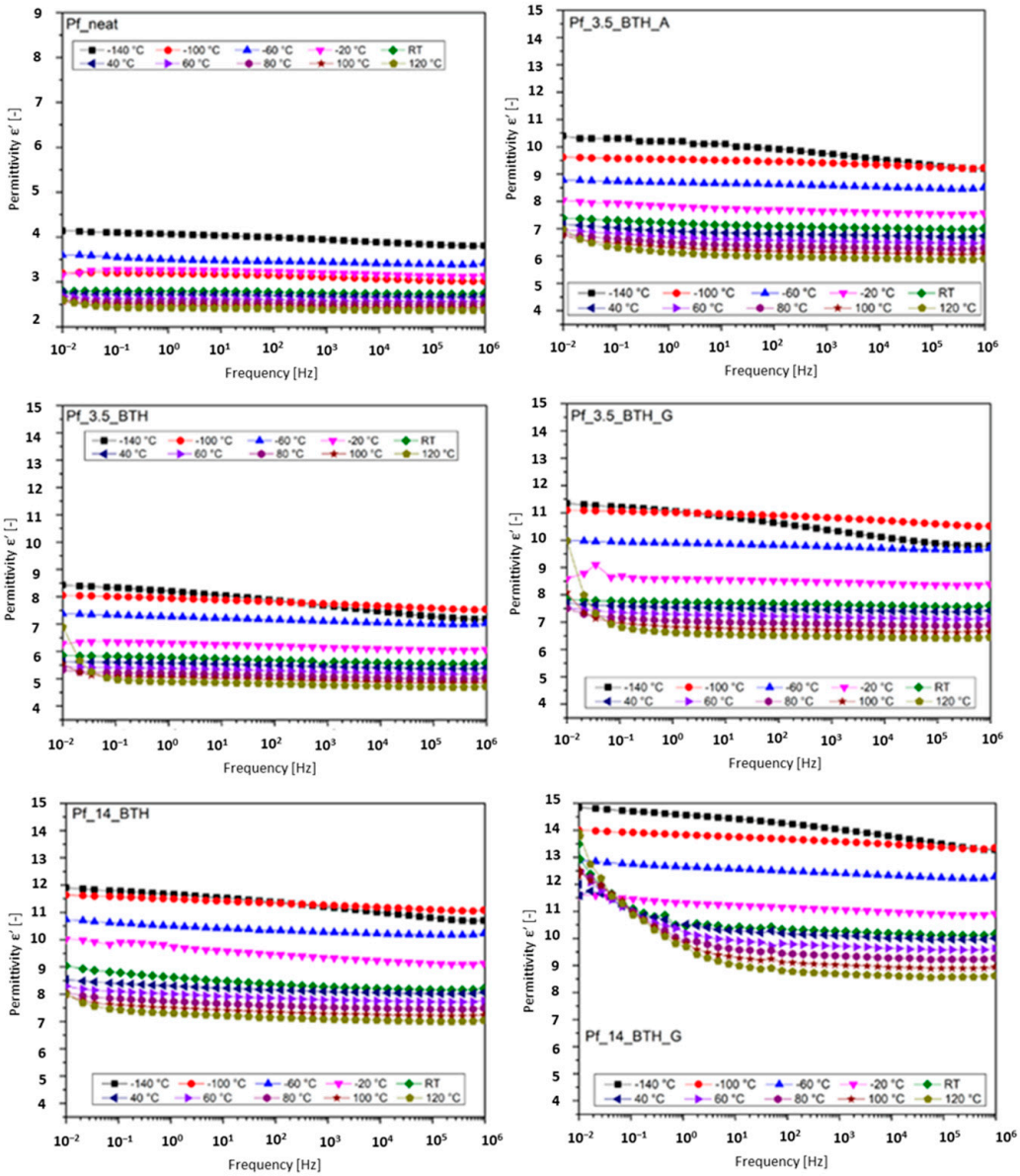

Figure 4. Frequency dependence of the real part of the permittivity for PDMS-based composites at various temperatures (from −140 °C to 120 °C).

Figure 5 shows the dissipation factor tan(δ) frequency and temperature dependence of all samples. This parameter is a common criterion for evaluating the performance of materials in terms of energy losses. The fact that the dielectric constant ε′ is not really affected by frequency does not distort our interpretation of the frequency change in tan(δ). Higher values of tan(δ) indicate greater dielectric losses in the polarization process. For all samples, tan(δ) has low values (<0.01) from 10^6 Hz down to 10^2 Hz. The significant increase in tan(δ) as the frequency decreases is a consequence of the AC conductivity of electric charges at long distances, which becomes dominant in the material at low frequencies. Mathematically, this AC conductivity is an imaginary term that adds to the dielectric losses. In the frequency range explored here, this AC conductivity becomes more pronounced, especially with increased temperature. At lower filler concentrations, functionalization seems beneficial for both tan(δ) and dielectric loss, likely due to a stronger particle–matrix interface. However, at room temperature (RT) at higher filler concentrations (Pf_14_BTH and Pf_14_BTH_G), tan(δ) becomes higher at lower frequencies. This is consistent with the higher SSA and blocking of electric charges at these interfaces. It is possible that an increase in AC conductivity within these clusters contributes to the rise in losses. The addition of fillers slightly reduces the overall loss factor, and low-frequency polarization occurs at higher frequencies compared to the neat matrix. This phenomenon becomes more pronounced with increasing temperature [42]. Furthermore, particle functionalization also influences the results. The effects of MWS (interfacial interaction) in G-functionalized samples become more apparent and occur at higher frequencies compared to the samples with bare particles, confirming the role of the interface in modulating dielectric response [18]. This suggests concurrent dipolar polarization, as functionalizing agents contain polar groups in their molecular structure. In addition to that, the behavior of Pf_3.5_BTH_A is similar to that of its G-functionalized counterpart. However, despite all these comments, the dielectric loss tangent at room temperature remains low for all composites, indicating that most of the electric energy can be converted into mechanical energy with minimal energy dissipation.

It is worth discussing the effect of temperature on the loss factor. At low temperatures, the dielectric loss is minimal and remains on the order of magnitude of 10^{-2} [43]. As temperature increases, the dielectric loss also increases due to higher thermal excitation. Conversely, at temperatures below −60 °C and −100 °C, the dielectric loss is lower [43]. This reduction can be attributed to the semi-crystalline nature of PDMS below −40 °C, where reduced chain mobility due to crystallization leads to lower losses. It is worth noting that the loss tangent at −140 °C consistently remains higher at high frequencies compared to the base value. The trend of tan(δ) is influenced by the polymeric matrix, as different relaxation mechanisms are activated at various temperatures and frequencies. At very low temperatures, the increase in dielectric loss (or tan δ) for the neat matrix at low frequency is due to α-relaxation mechanisms (polymeric chain re-arrangement) [43], while at higher temperatures, other phenomena like MWS and β-relaxation come into play [50]. As the temperature rises and surpasses the glass transition temperature (T_g), molecular chains exhibit more movement and orientation, resulting in visible manifestations of the relaxation process in the dielectric spectrum. In order to better understand this evolution of the dissipation factor, which must be analyzed with caution as it is impacted by both the change in frequency and in temperature of the dielectric constant and dielectric losses, to which must be added the term of long-distance electrical conduction, particularly at low frequencies, let us analyze the behavior of AC conductivity.

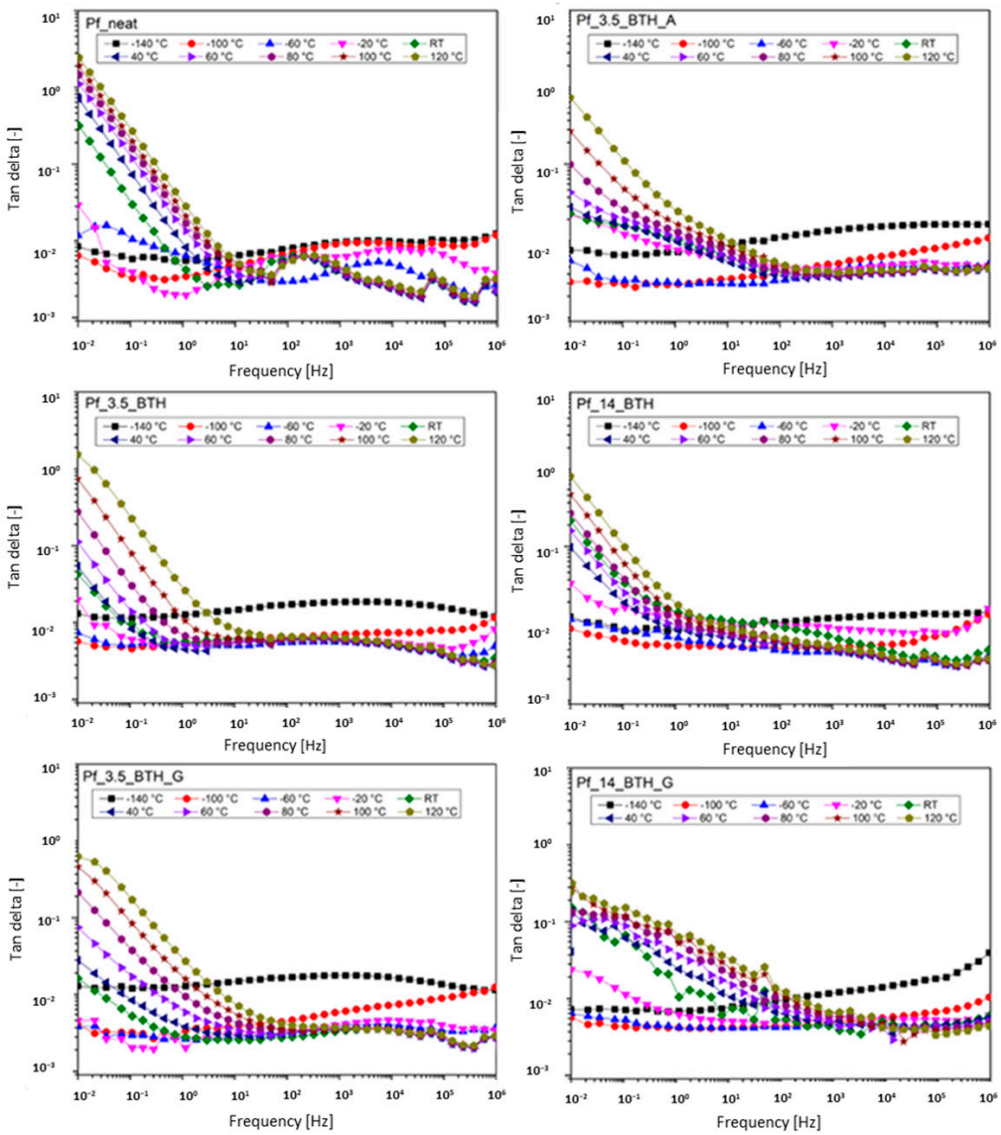

Figure 5. Frequency dependence of the dissipation factor tan(δ) for PDMS-based composites at various temperatures (from −140 °C to 120 °C).

AC conductivity trends were analyzed through DS measurements, indicating that all composites exhibit insulating properties. Figure 6 depicts the AC conductivity trends of the samples as a function of frequency and temperature. The observed behavior aligns with the universal Jonscher law ($\sigma_{ac}(\omega) = \sigma_{dc} + A\omega$n,), where the conductivity (σ_{ac}) in the AC regime follows a nearly linear relationship (on a log-log scale) from 10^{-8} to 10^{-14}–10^{-15} S/cm across the frequency range of 10^{6} Hz to 10^{-2} Hz. At low frequencies, a frequency-independent plateau is observed in most samples, indicating the presence of long-range electric AC conductivity (impacting the trend observed on the dissipation factor in this frequency range, see Figure 5). The nanocomposites' AC conductivity is strongly influenced by frequency and temperature, with a decrease in AC conductivity at lower frequencies due to dipole polarization or interfacial polarization (MWS polarization) [42]. Neat PDMS exhibits a prominent plateau at low frequencies (<100 Hz), particularly at higher temperatures, while the plateau diminishes with increasing filler, and it almost disappears when the particles are functionalized. Temperature also affects conductivity, with a plateau observed at higher temperatures (below 10 Hz) indicating a DC-conductivity component associated with long-range moving charges [43]. This effect is more pronounced in Pf_neat, reflecting the thermally activated nature of AC conductivity and the increase in DC bulk

conductivity [43]. The small increase in the room temperature conductivity can be linked to the introduction of ceramic fillers: at 1 kHz, the conductivity value is $5.2 \cdot 10^{-12}$ S/cm for Pf_neat and increases to $6.6 \cdot 10^{-11}$ S/cm and to $2.6 \cdot 10^{-11}$ S/cm, respectively, for Pf_3.5_BTH and Pf_14_BTH. When the filler concentration increases, the interfacial polarization also increases, leading to an increase in AC conductivity that may be caused by ion hopping in the polymer chain. However, despite the higher conductivity of the filler compared to the neat matrix, the addition of NPs does not significantly impact the final AC conductivity values. Functionalizing agents also influence AC conductivity, enhancing interfacial polarization. The presence of organosilanes at the matrix–particle interface can lead to charge accumulation, resulting in higher AC conductivity. RT AC conductivity at 1 kHz of the G-functionalized sample (Pf_3.5_BTH_G) is around $1.2 \cdot 10^{-11}$ S/cm which is almost six times higher with respect to that of the bare counterpart (Pf_3.5_BTH). Furthermore, with the polar functionalizing agents, a shoulder is observed rather than a plateau with an onset of around 10 Hz. This is particularly evident in the Pf_14_BTH_G sample. The situation is similar for the A-functionalized samples (Pf_3.5_BTH_A); moreover, the molecular structure of the functionalizing agent, with the presence of conductive PEO units in its chain, can affect the AC conductivity behavior, acting as long-range charge carriers and forming a more conductive path going through the filler network. A similar behavior was reported by Guan et al. [18] using carbon-nanotube-functionalized BT particles in a PDMS matrix. Let us analyze the low-frequency behavior of AC conductivity in more detail. Pf_neat is an RTV-type silicone with a platinum catalyst (manufacturer's data). Generally, mechanical reinforcement fillers (usually fumed silica) are incorporated into the PDMS matrix. These fillers, combined with the polymer chains, form interfacial zones where polarization mechanisms occur. It should be noted that for temperatures below the melting point (<−30 °C), no plateau is observable in the low frequencies. The polymer is semi-crystalline at these temperatures and the polymer chains are therefore more constrained, which does not favor conduction mechanisms, despite the rubbery nature of the material for our measurements above −100 °C. Slightly above −30 °C, at the lowest frequencies, we can see the beginning of a plateau in the measurement at −20 °C, at which point the polymer matrix has become amorphous or quasi-amorphous. At room temperature and above, long-distance charge conduction, with blocking at the interfaces with silica or movement in the silica clusters, results in a plateau in conduction at low frequencies, exacerbated by temperature. The addition of BTH charges does not degrade this low-frequency conductivity, and may even improve it slightly, probably by restricting the movement of the polymer chains. Indeed, for example, it can be seen that the conductivity plateau is less spread out in frequency for Pf_14_BTH in comparison with Pf_neat. Functionalization brings some change to this plateau, but nevertheless without significant change. The plateau, although slightly more spread out in frequency, is forced to curve downward. This curvature, although relatively slight, but visible in particular for Pf_14_BTH_G, is indeed the signature of a pronounced interfacial polarization mechanism, as already mentioned.

3.2.2. Breakdown Strength

Understanding and improving the breakdown strength of silicone elastomers has been the subject of several interesting studies over the past ten years [53–56]. The evaluation of the breakdown strength of PDMS-based composites was conducted, and the corresponding outcomes are presented in Table 2. It is worth noting that pure $BaTiO_3$ usually has a breakdown strength in the range 1–10 kV/mm [57], that, in some cases, with the proper doping, microstructure, and synthesis route, can go up to excellent values of 35–40 kV/mm [58]. The breakdown strength of unmodified and G-functionalized samples ranges from 33.0 to 40 kV/mm, depending upon filler loading and the presence of the

functionalizing agent. For neat PDMS, values are in the range 33.8 ± 5.4 kV. At low filler loading (3.5%), there is a minor increase in the breakdown strength discernible for bare particles. In contrast, Pf_3.5_BTH_G exhibits a pronounced increase of +18.0% in E_{BD} relative to neat PDMS. Nonetheless, a distinct scenario emerges in the context of samples with elevated loading (14%vol) wherein the mean breakdown strength aligns closely with that of neat PDMS. This is attributed to the diminished homogeneity characteristic of highly loaded samples, marked by the presence of sizable particle agglomerates acting as defects and inhomogeneities, thereby limiting the beneficial impact of particle incorporation. A-functionalized films, on the other hand, register an E_{BD} value of 42.1 kV/mm, signifying a notable increment of +24.5% compared to neat PDMS. This enhancement can be ascribed to the combined effect of improved particle dispersibility, defect mitigation, and the formation of tailored particle–matrix interfaces. Primarily, improved particle dispersibility due to functionalization results in more homogeneous composites devoid of defects, voids, and substantial agglomerations. Moreover, the polar functional groups introduced via G and A functionalization may act as shallow charge traps, effectively delaying dielectric breakdown by impeding charge mobility at the interface. While the functionalized samples show increased AC conductivity, likely due to interfacial polarization and enhanced dipolar mobility, this behavior does not necessarily reflect increased DC leakage currents. Rather, it may indicate more active interfacial regions, which are also involved in charge trapping mechanisms that stabilize the dielectric response under high field conditions [59–61].

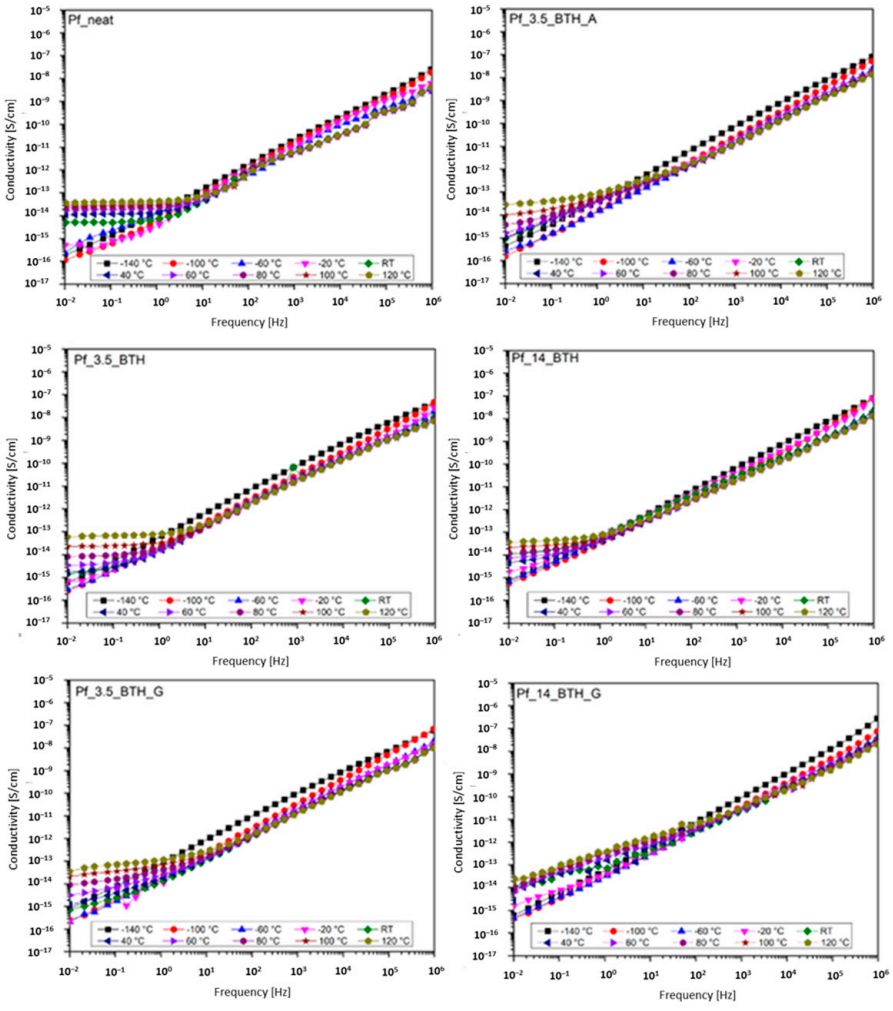

Figure 6. Frequency dependence of AC conductivity values for PDMS-based composites at various temperatures (from −140 °C to 120 °C).

Table 2. Breakdown strength for PDMS-based composite films with their relative standard deviation and the percentage difference with respect to the neat matrix.

Sample	E_{BD} [kV/mm]	Δ (Neat)
Pf_neat	33.8 (5.4)	-
Pf_3.5_BTH	34.6 (6.1)	+2.4%
Pf_3.5_BTH_G	39.9 (6.9)	+18.0%
Pf_14_BTH	33.0 (5.2)	−2.4%
Pf_14_BTH_G	34.8 (5.0)	+2.9%
Pf_3.5_BTH_A	42.1 (6.8)	+24.5%

3.2.3. Theoretical Energy Density Evaluation

The dielectric constant and breakdown strength values were used to estimate the theoretical upper limit of electrostatic energy density that can be stored in the composites using the standard relation $U = 1/2\varepsilon_0\varepsilon' E_{BD}^2$, where ε_0 represents the vacuum permittivity, ε' denotes the relative permittivity (chosen as reference for a frequency of 1 kHz), and E_{BD} represents the dielectric strength of the material. Results are summarized in Table 3. Neat PDMS shows an energy density of 29 mJ/cm^3. The addition of BTH NPs increases this value significantly. At 3.5%vol, bare particles (Pf_3.5_BTH) more than double the energy density, and at higher loadings, the dielectric constant further increases, though gains are limited by a drop in the breakdown strength. The most notable improvements are achieved at low filler content with functionalized NPs. Pf_3.5_BTH_G and Pf_3.5_BTH_A reach energy densities of over 100 mJ/cm^3—up to a 296% increase over neat PDMS. This is due to both enhanced NP dispersion and hybrid interface engineering via organosilane functionalization, which helps to maintain high permittivity while minimizing the breakdown losses. At higher filler loadings, namely at 14%vol, the presence of agglomerates limits the gain in permittivity by reducing the dielectric breakdown strength. Therefore, the results suggest that a low filler content with optimized interface chemistry is the ideal solution for achieving the greatest advantage in energy density. The values in Table 3 are comparable to or better than those reported in the literature for higher ceramic loadings [62–65], which highlights the effectiveness of properly designing hybrid interfaces in polymer nanocomposites for energy storage applications. The values of energy density found in this work are theoretically aligned with those found in the literature for silicone $BaTiO_3$ composites, ranging from 0.05 to 0.1 J/cm^3 [65]. However, it is worth nothing that this study merely aims to point out the potential behind the use of functionalizing agents; the real value depends on several factors, such as frequency, conversion yield, measuring conditions, and so on. Accordingly, the theoretical energy density was calculated at the standard reference frequency of 1 kHz, widely used in the literature. All these limitations are overestimating the energy density but provide a reasonable value for the maximum energy storage potential of these nanocomposites.

Table 3. Summary of dielectric constant, breakdown strength, and maximum theoretical energy density for PDMS-based composite films.

Sample	ε_r (1 kHz)	E_{BD} [kV/mm]	U [mJ/cm^3]/Δ(%)
Pf_neat	2.8	33.8	28/-
Pf_3.5_BTH	5.5	34.6	58/+107%
Pf_3.5_BTH_G	7.6	39.9	107/+282%
Pf_3.5_BTH_A	7.1	42.1	111/+296%
Pf_14_BTH	8.1	33.0	78/+178%
Pf_14_BTH_G	10.3	34.8	110/+294%

3.2.4. Effect of Stretching

Preliminary tests were performed to assess the electromechanical stability of the produced samples. Figure 7A shows the trend of the real part of the permittivity as a function of the frequency for the composites subjected to uniaxial stretching (λ = 2). In general, stretching leads to a decrease in the dielectric constant for all filled samples, while the neat PDMS matrix remains unaffected, aligning with previous research [66–68]. The extent of the reduction is smaller in the composites with functionalized fillers, especially those using APEOPTES, indicating a more stable dielectric response under mechanical deformation. In stretched samples, the permittivity decrease is likely influenced by changes in the polymer chain orientation and particle–matrix interactions, but these effects are less pronounced when the filler–matrix interfaces are properly engineered through NP functionalization. The AC conductivity trends (Figure 7B) remain generally similar between the stretched and unstretched samples. However, Pf_3.5_BTH_G and Pf_3.5_BTH_A show increased AC conductivity under stretching at low frequencies, which could be due to an orientation of the polar functional groups at the particle surface, creating more favorable pathways for charge transport [69–71]. Stretching also impacts the dielectric breakdown strength, as summarized in Table S2. A slight improvement is observed in most of the composites, with the greatest increase in Pf_14_BTH_G, which reaches 45.5 kV/mm—an increase of over 30% compared to its unstretched counterpart. This improvement is attributed to a combination of matrix stiffening and the stabilizing effect of the hybrid interface. Despite the drop in permittivity, the samples with functionalized fillers still retain relatively high energy densities under stretching, suggesting that the hybrid interface also supports resilience under mechanical deformation as shown in Table S2. However, the influence of stretching on the dielectric constant remains a complex issue: various factors like stretching ratio, initial/final thickness, electrode type, and measurement technique significantly impact the observed behavior [67]. The different mechanisms and their dependence on the factors mentioned above will be the subject of further studies.

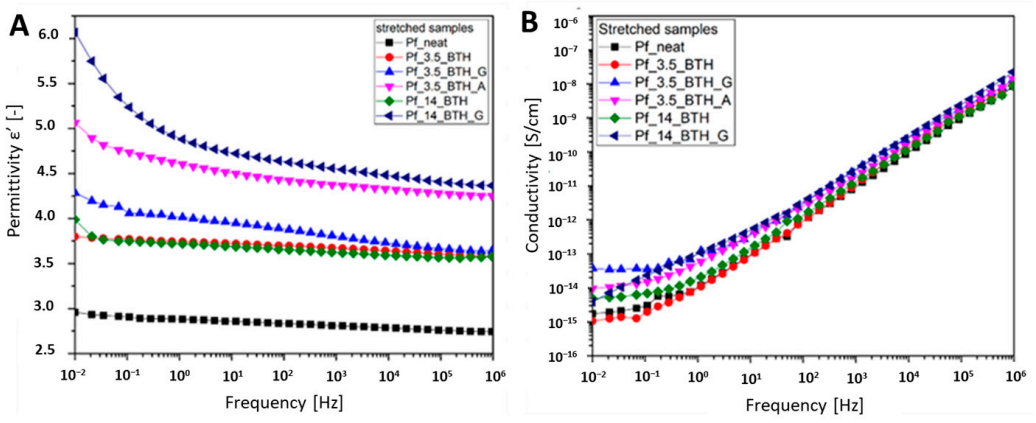

Figure 7. (**A**) Real part of permittivity for PDMS-based films as a function of the frequency. Samples were stretched with a stretching ratio of =2. (**B**) Room temperature AC of PDMS-based films as a function of the frequency range.

4. Conclusions

This study investigated the impact of BTH powder loading and functionalization on the dielectric properties of PDMS-based composites. The addition of BTH powders resulted in an increase in permittivity, especially at low frequencies, due to interfacial polarization. However, the relationship between filler quantity and dielectric constant was not linear, likely due to the formation of particle agglomerates at high filler contents. The design of hybrid interfaces through surface functionalization with organosilanes was proved to

be a simple but effective route to optimize composites' performance. In fact, functionalization improved permittivity by activating polarization mechanisms and improving particle dispersibility, leading to more homogeneous samples with extensive interfaces. The presence of polar groups in the functionalizing agents facilitated dipolar polarization of the silanes and promoted matrix–filler interactions. Engineering the particle–matrix hybrid interfaces affected the measured properties, being, for example, beneficial for reducing dielectric loss at low filler concentrations. Particularly notable is the use of APEOPTES, a novel silane functionalizing agent containing PEO chains, which outperformed GPTMS in several aspects. The film prepared with NPs functionalized with APEOPTES exhibited remarkable dielectric properties, including high permittivity, enhanced dielectric strength, and theoretical energy density values up to 111 mJ/cm^3 at just 3.5%vol filler loading. These improvements are attributed to the unique molecular structure of APEOPTES, which promotes both compatibility with the PDMS matrix and the formation of efficient interfaces capable of supporting charge trapping and interfacial polarization. The presence of polar organosilanes as functionalizing agents resulted in shoulder-like behavior in the AC conductivity curve, suggesting the creation of localized conductive pathways. Dielectric breakdown strength also improved thanks to functionalization, especially when using low filler loadings. In fact, at higher filler contents, the positive effects of functionalization were diminished by the presence of particle agglomerates. Preliminary tests on stretched samples confirmed the robustness of all composites, which maintained high dielectric performance, further supporting the relevance of interface engineering in applications requiring mechanical flexibility. Overall, this work underscores the importance of hybrid interface design as a straightforward and scalable strategy to achieve high dielectric performance of PDMS-based composites, while limiting the amount of ceramic nanoparticles, thus preserving the properties of the elastomer. The successful use of APEOPTES as a functionalizing agent offers new opportunities for tailoring interfacial chemistry in ceramic–elastomer systems and suggests broader applicability to other polymeric matrices.

Supplementary Materials: The following supporting information can be downloaded at: https://www.mdpi.com/article/10.3390/jcs10010058/s1, Figure S1: Scheme of the molecular structure of the used organosilanes, respectively, GPTMS, G (left) and APEOPTES, A (right); Figure S2: Homemade apparatus for sample stretching (left) and Cu-covered epoxy substrates for the testing; Figure S3: Setup for the measurement of the dielectric breakdown strength (left), homemade cell for evaluating breakdown strength of the films (right); Figure S4: Thermogravimetric curves of PDMS-based composites. The arrow indicates the shifting towards higher temperatures of the inflexion point from bare PDMS to PDMS composites; Figure S5: FTIR spectra of PDMS-based composites in the range 4000–550 cm^{-1}; Table S1: Decomposition temperatures of PDMS-based composites; Table S2: Summary of dielectric constant, dielectric breakdown value, and energy density for stretched composites.

Author Contributions: Conceptualization, N.Z. and S.D.; methodology, N.Z., A.S. and S.D.; validation, N.Z., A.S. and S.D.; formal analysis, N.Z.; investigation, N.Z.; resources, A.S., A.P., M.F. and S.D.; data curation, N.Z.; writing—original draft preparation, N.Z.; writing—review and editing, N.Z., A.S., A.P., M.F. and S.D.; visualization, N.Z.; supervision, A.P., M.F. and S.D.; funding acquisition, A.P., M.F. and S.D. All authors have read and agreed to the published version of the manuscript.

Funding: This work was performed in the frame of the program Departments of Excellence 2023–2027 (DII-UNITN)—Italian Ministry of University and Research (MUR).

Data Availability Statement: Data available upon request to the authors.

Conflicts of Interest: The authors declare no conflicts of interest.

Abbreviations

The following abbreviations are used in this manuscript:

PDMS	Polydimethylsiloxane
NPs	Nanoparticles
BT	$BaTiO_3$
BTH	Hydrothermal Barium Titanate
GPTMS (G)	3-glycidyloxypropyltrimethoxysilane
APEOPTES (A)	2-[acetoxy(polyethylenoxy)porpyl]triethoxysilane
SEM	Scanning Electron Microscopy
EDXS	Energy Dispersive X-Ray Spectroscopy
TGA	Thermogravimetric Analysis
DS	Dielectric Spectroscopy
E_{BD}	Electric Breakdown
MWS	Maxwell–Wagner–Sillars
PEO	Polyethyleneoxide
PEG	Polyethyleneglycole
RT	Room Temperature
AC	Alternating Current
DC	Direct Current

References

1. Yang, Z.; Zhou, S.; Zu, J.; Inman, D. High-Performance Piezoelectric Energy Harvesters and Their Applications. *Joule* **2018**, *2*, 642–697. [CrossRef]
2. Fan, F.; Tang, W.; Wand, Z. Flexible Nanogenerators for Energy Harvesting and Self-Powered Electronics. *Adv. Mater.* **2016**, *28*, 4283–4305. [CrossRef]
3. Stuber, V.; Deutz, D.; Bennet, J.; Cannel, D.; de Leeuw, D.; van der Zwaag, S.; Groen, W. Flexible Lead-Free Piezoelectric Composite Materials for Energy Harvesting Applications. *Energy Technol.* **2019**, *7*, 177–185. [CrossRef]
4. Moretti, G.; Rosset, S.; Vertechy, R.; Anderson, I.; Fontana, M. A review of Dielectric Elastomer Generator System. *Adv. Intell. Syst.* **2020**, *2*, 2000125. [CrossRef]
5. Yu, X.; Ji, Y.; Zhang, K.; Shen, X.; Zhang, S.; Xu, M.; Le, X. Ferroelectric Nanomaterials for Energy Harvesting and Self-Powered Sensing Application. *Adv. Sens. Res.* **2024**, *3*, 2400049. [CrossRef]
6. Tan, Y.; Gao, H.; Deng, J.; Lu, L.; Yao, L.; Pan, Z.; Deng, Q. High-Energy-Storage Dielectric Performance of Sandwich PI-based Composite over a Wide Temperature Range. *J. Phys. Chem. C* **2023**, *128*, 50–57. [CrossRef]
7. Barber, P.; Balasubramanian, S.; Anguchamy, Y.; Gong, S.; Wibowo, A.; Gao, H.; Ploehn, H.; Loye, H.-C. Polymer composite and nanocomposite dielectric materials for pulse power energy storage. *Materials* **2009**, *2*, 1697–1733. [CrossRef]
8. Romasanta, L.; Lopez-Manchado, M.; Verdejo, R. Increasing the performance of dielectric elastomers actuators: A review from the materials perspective. *Prog. Polym. Sci.* **2015**, *51*, 188–211. [CrossRef]
9. AlTowireb, S.; Goumri-Said, S. Core-Shell structures for the enhancement of energy harvesting in piezoelectric Nanogenerators: A review. *Sustain. Energy Technol. Assess.* **2023**, *55*, 102982. [CrossRef]
10. Abinnas, N.; Baskaran, P.; Harish, S.; Ganesh, R.; Navaneethan, M.; Nisha, K.; Ponnusamy, S.; Muthamizhchelvan, C.; Ikeda, H.; Hayakawa, Y. 0.8V nanogenerator for mechanical energy harvesting using bismuth titanate-PDMS nanocomposites. *Appl. Surf. Sci.* **2017**, *418*, 362–368. [CrossRef]
11. Nayak, S.; Chaki, T.; Khastgir, D. Development of Poly(dimethylsiloxane)/$BaTiO_3$ Nanocomposites as Dielectric Material. *Adv. Mater. Res.* **2014**, *622–623*, 897–900.
12. Nayak, S.; Chaki, T.; Khastgir, D. Development of Flexible Piezoelectric Poly(dimethylsiloxane)-$BaTiO_3$ Nanocomposites for Electrical Energy Harvesting. *Ind. Eng. Chem. Res.* **2014**, *53*, 14982–14992. [CrossRef]
13. Li, S.; Yin, G.; Chen, G.; Li, J.; Bai, S.; Zhong, L.; Zhang, Y.; Lei, Q. Short-term breakdown and long-term failure in nanodielectrics: A review. *IEEE Trans. Dielectr. Electr. Insul.* **2010**, *17*, 1523–1535. [CrossRef]
14. Zhou, Z.; Du, X.L.J.; Yao, L.; Zhang, Z.; Yang, H.; Zhang, Q. Coupling of interface effects and porous microstructures in translucent piezoelectric composite for enhanced energy harvesting and sensing. *Nano Energy* **2021**, *84*, 105895. [CrossRef]
15. Cho, S.; Lee, J.; Jang, J. Enhanced Crystallinity, Dielectric, and Energy Harvesting Performance of Surface-Treated Barium Titanate Hollow Nanospheres/PVDF Nanocomposites. *Adv. Mater. Interfaces* **2015**, *2*, 1500098. [CrossRef]

16. Dalle Vacche, S.; Oliveira, F.; Leterrier, Y.; Michaud, V.; Damjanovic, D.; Manson, J.-A.E. Effect of silane coupling agent on the morphology, structure, and properties of poly(vinylidene fluoride-trifluoroethylene)/$BaTiO_3$ composites. *J. Mater. Sci.* **2014**, *49*, 4552–4564. [CrossRef]
17. Domrzalski, J.; Stevens, T.; Van Ginhoven, R.; Fritzsching, K.; Walfer, B.; Johnson, E.; Lewis, R.; Vreeland, E.; Pearce, C.; Vargas, D.; et al. Surface Functionalized Barium Titanate Nanoparticles: A Combined Experimental and Computational Study. *ECS J. Solid State Sci. Technol.* **2022**, *11*, 063006. [CrossRef]
18. Guan, S.; Tang, Y.; Song, S.; Liu, H.; Zhao, S. Influence of inter structure of $BaTiO_3$-carbon nanotube hybrid particles on the dielectric properties of PDMS nanocomposites. *Mater. Sci. Eng. B* **2021**, *271*, 115280. [CrossRef]
19. Zafar, R.; Gupta, N. Estimation of interface properties in epoxy-based barium titanate nanocomposites. *J. Phys. Commun.* **2021**, *5*, 075003. [CrossRef]
20. Zafar, R.; Gupta, N. Pre-processing of $BaTiO_3$ nanofillers in improving dielectric response of epoxy nanocomposites at higher filler concentrations. In *Proceedings of the 2017 IEEE Conference on Electrical Insulation and Dielectric Phenomenon (CEIDP), Fort Worth, TX, USA, 22–25 October 2017*; IEEE: New York, NY, USA, 2017; pp. 477–480.
21. Yang, D.; Ni, Y.; Xu, Y.; Kong, X.; Feng, Y.; Zhanf, L. Nitrile-butadiene rubber composites with improved electromechanical properties obtained by modification of $BaTiO_3$ with co-deposited catechol/polyamine and silane grafting. *Polymer* **2019**, *183*, 121813. [CrossRef]
22. Zhu, S.; Guo, J.; Zhang, J. Enhancement of mechanical strength associated with interfacial tension between barium titanate and acrylonitrile-butadiene rubber with different acrylonitrile contents by surface modifications. *J. Appl. Polym. Sci.* **2017**, *135*, 45936. [CrossRef]
23. Ma, P.; Kim, J.-K.; Tang, B. Effects of silane functionalization on the properties of carbon nanotube/epoxy nanocomposites. *Compos. Sci. Technol.* **2007**, *67*, 2965–2972. [CrossRef]
24. Yang, D.; Ruan, M.; Huang, S.; Wu, Y.; Li, S.; Wang, H.; Ao, X.; Liang, Y.; Guo, W.; Zhang, L. Dopamine and silane functionalized barium titanate with improved electromechanical properties for silicone dielectric elastomers. *RSC Adv.* **2016**, *6*, 90172–90183. [CrossRef]
25. Thames, S.; Panjnani, K. Organosilane Polymer Chemistry: A Review. *J. Inorg. Organomet. Polym.* **1996**, *6*, 59–94. [CrossRef]
26. Shanmugasundram, H.P.P.V.; Jayamani, E.; Soon, K.H. Dielectric bionanocomposites with organoclay and silane-treated conductive fillers for reduced dielectric relaxation times. *Mater. Chem. Phys.* **2025**, *337*, 130569. [CrossRef]
27. Moharanaa, S.; Mishraa, M.; Beherab, B.; Mahalinga, R. Enhanced Dielectric Properties of Polyethylene Glycol (PEG) Modified $BaTiO_3$ (BT)-Poly(vinylidene fluoride) (PVDF) Composites. *Polym. Sci.* **2017**, *59*, 405–415. [CrossRef]
28. Zamperlin, N.; Ceccato, R.; Fontana, M.; Pegoretti, A.; Chiappini, A.; Dire', S. Effect of Hydrothermal Treatment and Doping on the Microstructural Features of Sol-Gel Derived $BaTiO_3$ Nanoparticles. *Materials* **2021**, *14*, 4345. [CrossRef]
29. Zamperlin, N.; Bottacini, A.; Callone, E.; Pegoretti, A.; Fontana, M.; Dire', S. Barium Titanate Functionalization with Organosilanes: Effect on Particle Compatibility and Permittivity in Nanocomposites. *Molecules* **2022**, *27*, 6499. [CrossRef]
30. Mandal, S.; Hou, Y.; Wang, M.; Anthopoulos, T.; Choy, K. Surface Modification of Hetero-phase Nanoparticles for Low-Cost. *ACS Appl. Mater. Interfaces* **2023**, *15*, 7371–7379. [CrossRef]
31. Guo, C.; Fuji, M. Effect of silicone coupling agent on dielectric properties of barium/silicone elastomer composites. *Adv. Powder Technol.* **2016**, *27*, 1162–1172. [CrossRef]
32. Wang, Y.; Wu, X.; Feng, C.; Zeng, Q. Improved dielectric properties of surface modified $BaTiO_3$/polyimide. *Microelectron. Eng.* **2016**, *154*, 17–21. [CrossRef]
33. Niranjana, V.; Ponnan, S.; Mukundan, A.; Prabu, A.; Wang, H.-C. Emerging Trends in Silane-Modified Nanomaterial–Polymer Nanocomposites for Energy Harvesting Applications. *Polymers* **2025**, *17*, 1416. [CrossRef]
34. Tang, X.; Zhang, Z.; Kumar, D.; Qu, Y.; Long, Y.; Xie, P.; Liang, G.; Wang, J.; Yang, Q.; Qi, X.; et al. Flexible Carbon Nanotubes/Polystyrene Membranous Composites Toward Ultraweakly and Frequency-Stable Negative Permittivity at kHz Region. *Eng. Sci.* **2023**, *24*, 920. [CrossRef]
35. Wu, H.; Zhang, Z.; Wang, C.; Abualnaja, K.; Abo-Dief, H.; Hou, Q.; Algadi, H.; Yin, R.; Liu, X.; Xie, P.; et al. Radio-frequency broadband epsilon-near-zero response in biocompatible silver nanoparticles/polystyrene films with three-dimensional honeycomb-like superstructures. *Adv. Compos. Hybrid Mater.* **2023**, *6*, 206. [CrossRef]
36. Samet, M.; Kallel, A.; Serghei, A. Maxwell-Wagner-Sillars interfacial polarization in dielectric spectra of composite materials: Scaling laws and applications. *J. Compos. Mater.* **2022**, *56*, 3197–3217. [CrossRef]
37. Beena, P.; Jayanna, H. Dielectric studies and AC conductivity of piezoelectric barium titanate ceramic polymer composites. *Polym. Polym. Compos.* **2019**, *27*, 619–625. [CrossRef]
38. Mathias, K.A.; Shivashankar, H.; Manohar Shankar, B.S.; Kulkarni, S.M. Influence of filler on dielectric properties of silicon rubber particulate composite material. *Mater. Today Proc.* **2020**, *33*, 5623–5627. [CrossRef]
39. Yang, J.; Deng, X.; Li, J.; Cai, Q.; Zhang, H.; Wang, L.; Su, K.; Zhang, G.; Wang, C. Broadband dielectric spectroscopy analysis of dielectric properties of barium titanate ceramics. *Adv. Mater. Res.* **2013**, *744*, 323–328. [CrossRef]

40. Hoshina, T.; Takizawa, K.; Li, J.; Kasama, T.; Kakemoto, H.; Tsurumi, T. Domain Size Effect on Dielectric Properties of Barium Titanate Ceramics. *Jpn. J. Appl. Phys.* **2008**, *47*, 7607–7611. [CrossRef]
41. Meddeb, A.; Ounaies, Z.; Lopez-Pamies, O. Interfacial effects on the electrical behavior of elastomer nanoparticulate composites. In *SPIE Smart Structures + Nondestructive Evaluation, Denver, CO, USA, 3–7 March 2019, 2019*; SPIE: Cergy-Pontoise, France, 2019; Volume 10968, p. 109680I.
42. Gonzalez, N.; dels Angels Culstal, M.; Tomara, G.; Psarras, G.; Riba, J.-R.; Armelin, E. Dielectric response of vulcanized natural rubber containing $BaTiO_3$ filler: The role of particle functionalization. *Eur. Polym. J.* **2017**, *97*, 57–67. [CrossRef]
43. Asandulesa, M.; Musteata, V.; Bele, A.; Dascalu, M.; Bronnikov, S.; Racles, C. Molecular dynamics of polysiloxane polar-nonpolar co-networks and blends studied by dielectric relaxation spectroscopy. *Polymer* **2018**, *149*, 73–84. [CrossRef]
44. Samet, M.; Boiteux, G.; Seytre, G.; Kallel, A.; Serghei, A. Interfacial polarization in composite materials with spherical fillers: Characteristics frequencies and scaling laws. *Colloid Polym. Sci.* **2014**, *292*, 1977–1988. [CrossRef]
45. Guo, H.; Zhang, C.; Zhang, N.; Jin, L.; Gao, Y.; Bai, J.; Zhao, H. Enhanced Electro-Actuation and Self-Healing Properties of Dielectric Elastomers by Introducing Ultrafine $BaTiO_3$ and Semi-Interpenetrating Macromolecules. *ACS Appl. Polym. Mater.* **2025**, *7*, 680–690. [CrossRef]
46. Wang, W.; Ren, G.; Zhou, M.; Deng, W. Preparation and Characterization of CCTO/PDMS Dielectric Elastomers with High Dielectric Constant and Low Dielectric Loss. *Polymers* **2021**, *13*, 1075. [CrossRef]
47. Gao, S.; Zhao, H.; Zhang, N.; Bai, J. Enhanced Electromechanical Property of Silicone Elastomer Composites Containing TiO_2@SiO_2 Core-Shell Nano-Architectures. *Polymers* **2021**, *13*, 368. [CrossRef]
48. Bosq, N.; Guigo, N.; Persello, J.; Sbirrazzuoli, N. Melt and glass crystallization of PDMS and PDMS silica nanocomposites. *Phys. Chem. Chem. Phys.* **2014**, *16*, 7830–7840. [CrossRef]
49. Utrera-Barrios, S.; Yu, L.; Skov, A. Revisiting the Thermal Transitions of Polydimethysiloxane (PDMS) elastomers: Addressing Common Misconceptions with Comprehensive Data. *Macromol. Mater. Eng.* **2025**, *310*, 2500075. [CrossRef]
50. Klonos, P. Crystallization, glass transition, and molecular dynamics in PDMS of low molecular weights: A calorimetric and dielectric study. *Polymer* **2018**, *159*, 169–180. [CrossRef]
51. Belovickis, J.; Macutkevic, J.; Svirskas, S.; Samulionis, V.; Banys, J.; Shenderova, O.; Borjanovic, V. Dielectric Spectroscopy of Polymer Based PDMS Nanocomposites with ZnO Nanoparticles. *Ferroelectrics* **2015**, *479*, 82–89. [CrossRef]
52. Fahmy, T.; Elzanaty, H. AC conductivity and broadband dielectric spectroscopy of a poly(vinyl chloride)/poly(ethyl methacrylate) polymer blend. *Bull. Mater. Sci.* **2019**, *42*, 220. [CrossRef]
53. Razak, A.H.A.; Yu, L.; Skov, A.L. Voltage-stabilised elastomers with increased relative permittivity and high electrical breakdown strength by means of phase separating binary copolymer blends of silicone elastomers. *RSC Adv.* **2017**, *7*, 17848. [CrossRef]
54. Kuroda, R.; Jeon, H.-G.; Ihori, H. Electrical treeing phenomena in two-layer silicone gel with different crosslinking degrees and its dielectric strength. *Electr. Eng. Jpn.* **2023**, *216*, e23437. [CrossRef]
55. Luo, M.; Zhou, Y.; Wang, R.; Cao, X.; Wang, Z. Enhanced dielectric breakdown strength and thermal conductivity of silicone gel composites with high-electron-affinity silicon Dioxide/Cationic Polymer/Nano-diamond. *Chem. Eng. J.* **2024**, *501*, 157623. [CrossRef]
56. Mateiu, R.V.; Yu, L.; Skov, A.L. Electrical breakdown phenomena of dielectric elastomers. In *SPIE Smart Structures + Nondestructive Evaluation, Portland, OR, USA, 25 March–29 June 2017*; SPIE: Cergy-Pontoise, France, 2017; Volume 10163, p. 1016328.
57. Gavrilenko, V.; Vidal, P.-E.; Kohler, T.; Raisson, R.; Guillemet-Fritsch, S.; Dufour, P.; Pecastaing, L. Breakdown strength study of barium titanate ceramics for power electronic applications. In *Proceedings of the 2024 IEEE 5th International Conference on Dielectrics, Toulouse, France, 30 June–4 July 2024*; IEEE: New York, NY, USA, 2024; pp. 1–4.
58. Liu, G.; Li, Y.; Guo, B.; Tang, M.; Li, Q.; Dang, J.; Yu, L.; Yu, K.; Yan, Y.; Wang, D.; et al. Ultrahigh dielectric breakdown strength and excellent energy storage performance in lead-free barium titanate-based relaxor ferroelectric ceramics via a combined strategy of composition modification, viscous polymer processing and liquid-phase sintering. *Chem. Eng. J.* **2020**, *398*, 125625. [CrossRef]
59. Yeung, C.; Vaughan, A. On the effect of nanoparticle surface chemistry on the electrical characteristics of epoxy-based nanocomposites. *Polymers* **2016**, *8*, 126. [CrossRef]
60. Li, S.; Xie, D.; Qu, G.; Yang, L.; Min, D.; Cheng, Y. Tailoring interfacial compatibility and electrical breakdown properties in polypropylene based composites by surface functionalized POSS. *Appl. Surf. Sci.* **2019**, *478*, 451–458. [CrossRef]
61. Mahtabani, A.; Rytoluoto, I.; Anyszka, R.; He, S.; Saarimaki, E.; Lahti, K.; Dierkes, W.; Blume, A. On the Silica Surface Modification and Its Effect on Charge Trapping and Transport in PP-Based Dielectric Nanocomposites. *ACS Appl. Polym. Mater.* **2020**, *2*, 3148–3160. [CrossRef]
62. Kim, T.; Lim, H.; Lee, Y.; Kim, B.-J. Synthesis of $BaTiO_3$ nanoparticles as shape modified filler for high dielectric constant ceramic–polymer composite. *RSC Adv.* **2020**, *10*, 29278–29286. [CrossRef] [PubMed]
63. Cai, C.; Chen, T.; Chen, X.Z.Y.-T.; Gong, X.-H.; Wu, C.-G.; Hu, T. Enhanced Electromechanical Properties of Three-Phased Polydimethylsiloxane Nanocomposites via Surface Encapsulation of Barium Titanate and Multiwalled Carbon Nanotube with Polydopamine. *Macromol. Mater. Eng.* **2021**, *306*, 2100046. [CrossRef]

64. Chen, Y.; Agostini, L.; Moretti, G.; Fontana, M.; Vertechy, R. Dielectric elastomer materials for large-strain actuation and energy harvesting: A comparison between styrenic rubber, natural rubber and acrylic elastomer. *Smart Mater. Struct.* **2019**, *28*, 114001. [CrossRef]
65. Banet, P.; Nouh, Z.; Chavanne, J.; Nhuyen, G.; Chikh, L.; Plesse, C.; Almanza, M.; Martinez, T.; Civet, Y.; Perriard, Y.; et al. Evaluation of dielectric elastomers to develop materials suitable for actuation. *Soft Matter* **2021**, *17*, 10786–10805. [CrossRef] [PubMed]
66. Tröls, A.; Kogler, A.; Baumgartner, R.; Kaltseis, R.; Keplinger, C.; Schwödiauer, R.; Graz, I.; Bauer, S. Stretch dependence of the electrical breakdown strength and dielectric constant of dielectric elastomers. *Smart Mater. Struct.* **2013**, *22*, 104012. [CrossRef]
67. Jean-Mistral, C.; Sylvestre, A.; Basrour, S.; Chaillout, J.-J. Dielectric properties of polyacrylate thick films used in sensors and actuators. *Smart Mater. Struct.* **2010**, *19*, 075019. [CrossRef]
68. Vu-Cong, T.; Nguyen-Thi, N.; Jean-Mistral, C.; Sylvestre, A. How does static stretching decrease the dielectric constant of VHB 4910 elastomer? In *SPIE Smart Structures + Nondestructive Evaluation, San Diego, CA, USA, 9 March–13 May 2014*; SPIE: Cergy-Pontoise, France, 2014; Volume 9056, p. 90561P.
69. Shantala, V.; Shobha Devi, S.; Murugendrappa, M. Synthesis, characterization and DC conductivity studies of polypyrrole/copper zinc iron oxide nanocomposites. *J. Asian Ceram. Soc.* **2017**, *5*, 227–234. [CrossRef]
70. Zhu, S.; Sun, H.; Lu, Y.; Wang, S.; Yue, Y.; Xu, X.; Mei, C.; Xiao, H.; Fu, Q.; Han, J. Inherently Conductive Poly(dimethylsiloxane) Elastomers Synergistically Mediated by Nanocellulose/Carbon Nanotube Nanohybrids toward Highly Sensitive, Stretchable, and Durable Strain Sensors. *ACS Appl. Mater. Interfaces* **2021**, *13*, 59142–59153. [CrossRef]
71. Xu, S.; Yu, W.; Jing, M.; Huang, R.; Zhang, Q.; Fu, Q. Largely Enhanced Stretching Sensitivity of Polyurethane/Carbon Nanotube Nanocomposites via Incorporation of Cellulose Nanofiber. *J. Phys. Chem. C* **2017**, *121*, 2108–2117. [CrossRef]